

PAPER • OPEN ACCESS

## Efficient in-line skyrmion injection method for synthetic antiferromagnetic systems

To cite this article: W L Gan *et al* 2018 *New J. Phys.* **20** 013029

View the [article online](#) for updates and enhancements.



## PAPER

## Efficient in-line skyrmion injection method for synthetic antiferromagnetic systems

## OPEN ACCESS

## RECEIVED

25 October 2017

## REVISED

30 November 2017

## ACCEPTED FOR PUBLICATION

12 December 2017

## PUBLISHED

22 January 2018

W L Gan , S Krishnia and W S Lew

School of Physical and Mathematical Sciences, Nanyang Technological University, 21 Nanyang Link, Singapore 637371, Singapore

E-mail: [wensiang@ntu.edu.sg](mailto:wensiang@ntu.edu.sg)**Keywords:** skyrmion, magnetic memory, spin-orbit torque, spin Hall effect, domain wallSupplementary material for this article is available [online](#)

Original content from this work may be used under the terms of the [Creative Commons Attribution 3.0 licence](#).

Any further distribution of this work must maintain attribution to the author(s) and the title of the work, journal citation and DOI.

**Abstract**

Although it has been proposed that antiferromagnetically-coupled skyrmions can be driven at extremely high speeds, such skyrmions are near impossible to inject with current methods. In this paper, we propose the use of DMI-induced edge magnetization tilting to perform in-line skyrmion injection in a synthetic antiferromagnetic branched nanostructure. The proposed method circumvents the skyrmion topological protection and lowers the required current density. By allowing additional domain walls (DWs) to form on the branch, the threshold injection current density was further reduced by 59%. The increased efficiency was attributed to inter-DW repulsion and DW compression. The former acts as a multiplier to the effective field experienced by the pinned DW while the latter allows DWs to accumulate enough energy for depinning. The branch geometry also enables skyrmions to be shifted and deleted with the use of only three terminals, thus acting as a highly scalable skyrmion memory block.

**1. Introduction**

Magnetic skyrmions are bubble-like magnetization configurations that exist in the nanometer length scale. Due to their many attractive attributes as a candidate for a universal memory, they have been at the center of much scientific endeavors [1–7]. However, a few persistent challenges hinder the realization of the skyrmionic memory. First of which is the presence of a skyrmion Hall effect which leads to a transverse motion of the skyrmion under an electric current. This behavior often leads to skyrmion annihilation at the nanowire edges and imposes a speed limit for skyrmions [1, 5, 8–12]. Secondly, as skyrmions are magnetically charged, they experience significant repulsion with each other [6]. This limits the skyrmion packing density and imposes a data density limit on any skyrmion-based memory device.

Although several solutions have been proposed to overcome these challenges, the switch to the use of a synthetic antiferromagnetic (SAF) medium for skyrmion motion have been shown to be more promising [10, 13]. In such systems, two skyrmions with opposite polarity but similar chirality are coupled antiferromagnetically across a heavy metal layer. In the SAF medium, the compensating magnetic moments of the top and bottom layers are insensitive to externally applied magnetic fields, resulting in single skyrmion injection becoming an almost impossible task. Research by Zhou Yan *et al* has shown that the vertical injection of spin-polarized current can create skyrmions [10]. However, even with a low interlayer exchange of  $-2 \text{ pJ m}^{-1}$ , spin current densities of at least  $700 \text{ MA cm}^{-2}$  are needed. The resulting Joule heating imposes a large thermal stress on the magnetic material, affecting both its spin configuration and its magnetic properties [14–17]. Consequently, the lack of a reliable method to inject single skyrmions remains a key challenge for the development of skyrmionic memory devices.

In this paper, we demonstrate a highly efficient, in-line and on-demand injection scheme for SAF-coupled skyrmions on a branched magnetic nanostructure. At the branch edges, the DMI-induced magnetization tilting was harnessed to create a chiral in-plane magnetization that allows spin-orbit torques (SOTs) to efficiently

**Table 1.** List of micromagnetic parameters used for numerical and analytical calculations.

Symbol	Quantity	Value
$M_{\text{sat}}$	Saturation magnetization	580 kA m <sup>-1</sup>
$K_{\text{u}}$	Uniaxial anisotropy	500 kJ m <sup>-3</sup>
$D$	Dzyaloshinskii–Moriya interaction strength	2 mJ m <sup>-2</sup>
$A$	Exchange stiffness	15 pJ m <sup>-1</sup>
$\alpha$	Damping parameter	0.1
$\xi$	Degree of non-adiabaticity	0.35
$\theta_{\text{SH}}$	Spin Hall angle	0.15

nucleate domains. The domains are then ejected from the branch and propelled into the nanowire to form a skyrmion. The energy-intensive depinning processes was found to be governed by inter-domain wall (DW) repulsion and compression which, in a SAF material, exhibit a spring-like behavior. The effect was exploited by the injection of an additional DW into the branch to further reduce the threshold injection current density by a third. Reversing the applied current, we show that the skyrmions are drawn towards the branch and deleted. Therefore, the proposed branched nanostructure can inject, shift, and delete skyrmions efficiently.

## 2. Methods

### 2.1. Micromagnetic model

The numerical simulation was performed with a modified version of the mumax3 micromagnetics solver. The solver evolves the magnetization in discrete time steps using the Landau–Lifshitz–Gilbert equation with added spin torque terms. The full equation is given by [37]:

$$\frac{\partial \vec{m}}{\partial t} = \frac{\gamma_0}{1 + \alpha^2} (\vec{m} \times \vec{B}_{\text{eff}} + \alpha (\vec{m} \times (\vec{m} \times \vec{B}_{\text{eff}}))) + \vec{\tau}_{\text{STT}} + \vec{\tau}_{\text{SHE}},$$

where  $\gamma_0$  is the electron gyromagnetic ratio,  $\alpha$  is the damping parameter and  $\vec{B}_{\text{eff}}$  is the effective field. To calculate the effective field, material parameters of Co/Pt multilayers are used as shown in table 1 [5, 6]. The synthetic ferromagnetic coupling models the use of a 0.4 nm Ruthenium spacer layer between the top and bottom magnetic layers with an interlayer exchange strength corresponding to 0.2 pJ m<sup>-1</sup> [35]. However, the magnetization dynamics was found to be insensitive to changes in the SAF coupling strength as long as the skyrmions remains coupled. In all simulations, cell sizes of  $1 \times 1 \times 0.4$  nm<sup>3</sup> were used. The Zhang-Li spin torque  $\vec{\tau}_{\text{STT}}$  and the spin Hall torque  $\vec{\tau}_{\text{SHE}}$  are expressed as [23, 37]:

$$\vec{\tau}_{\text{STT}} = \frac{1}{1 + \alpha^2} ((1 + \xi\alpha) \vec{m} \times (\vec{m} \times (\vec{j} \cdot \nabla) \vec{m}) + (\xi - \alpha) \vec{m} \times (\vec{j} \cdot \nabla) \vec{m}),$$

$$\vec{j} = \frac{\mu_B \mu_0 \dot{J}_a}{2e\gamma_0 M_{\text{sat}} (1 + \xi^2)} \hat{u},$$

$$\vec{\tau}_{\text{SHE}} = \frac{1}{1 + \alpha^2} \frac{\mu_B \theta_{\text{SH}} \dot{J}_a}{eM_s t} \vec{m} \times ((\hat{u} \times \hat{z}) \times \vec{m}),$$

where  $\xi$  is the degree of non-adiabaticity,  $\hat{u}$  is the current density unit vector,  $e$  the electronic charge,  $M_{\text{sat}}$  the saturation magnetization,  $\theta_{\text{SH}}$  is the spin Hall angle and  $t$  is the film thickness in the  $z$ -direction. The above implementation of  $\vec{\tau}_{\text{SHE}}$  was added to the source code of the solver used. The material parameters used for the micromagnetic calculations are listed in table 1. For the synthetic antiferromagnet stack, the Ru layer is assumed to not contribute to either DMI or SOT experienced by the magnetic layers as Ru/Co interfaces show a low spin-orbit coupling [38].

### 2.2. Current density modeling

The current density for the branched nanostructures were calculated using the DC current module in the COMSOL multiphysics software. The current densities stated were taken from the average current density in the device area shown in figure 2(b).

### 2.3 DW length calculation

In the calculation of the DW length, the following magnetization profile for the Néel wall was assumed [34],  $\theta(x) = 2 \tan^{-1} \left( \frac{e^{x/L} - 1}{e^{x/L} + 1} \right)$ , where  $\theta$  is the magnetization angle in the  $xz$ -plane. In this case,  $x$  is taken to be zero at

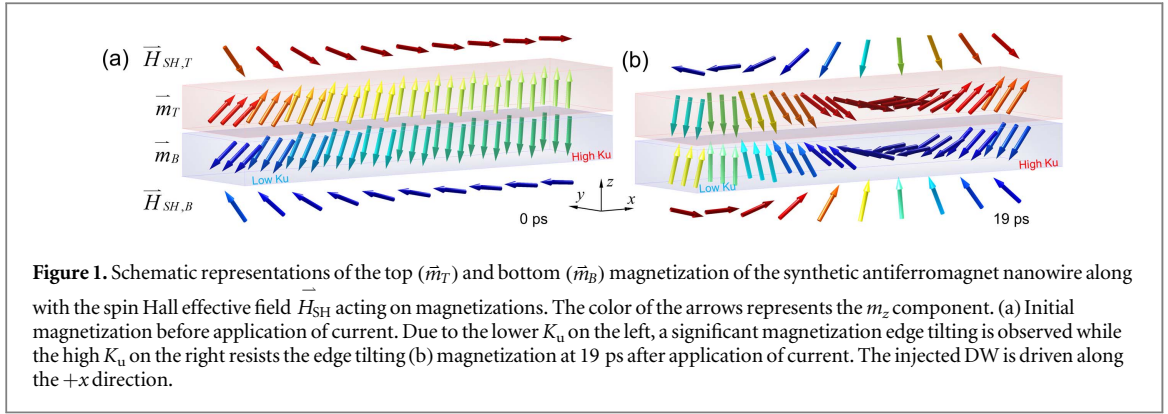


**Figure 1.** Schematic representations of the top ( $\vec{m}_T$ ) and bottom ( $\vec{m}_B$ ) magnetization of the synthetic antiferromagnet nanowire along with the spin Hall effective field  $\vec{H}_{SH}$  acting on magnetizations. The color of the arrows represents the  $m_z$  component. (a) Initial magnetization before application of current. Due to the lower  $K_u$  on the left, a significant magnetization edge tilting is observed while the high  $K_u$  on the right resists the edge tilting (b) magnetization at 19 ps after application of current. The injected DW is driven along the  $+x$  direction.

the center of the DW. The expression can be rearranged to show the out-of-plane magnetization component,  $m_z(x) = \tanh\left(\frac{x}{L}\right)$ . The position  $x$  which solves the equation was taken to be the start and end of the DW.

### 3. Spin orbit torque-induced in-line domain injection

SOTs have been the subject of many recent research endeavors due to their potential for efficient magnetization switching [18–22]. In particular, the spin accumulation at the heavy metal-ferromagnet interface due to the spin Hall effect has been found to be useful for magnetization switching. The effective field from the spin Hall effect for an electric current applied in the  $x$  direction is given by  $\vec{H}_{SH} = -\frac{\hbar\theta_{SH}j_a}{2\mu_0|e^-|M_s t} \vec{m} \times \hat{y}$  where  $\vec{m}$  is the magnetization,  $\theta_{SH}$  is the spin Hall angle,  $j_a$  is the applied current density and  $t$  is the thickness of the magnetic material [23]. To enable efficient SOT-induced magnetization switching in perpendicular magnetic anisotropy (PMA) materials, the  $z$ -component in  $\vec{H}_{SH}$  should be maximized by having large  $x$ -magnetization ( $m_x$ ) [24–26]. It is then convenient to take advantage of the inherent edge magnetization tilting effect due to the DMI to produce a  $m_x$ .

In PMA ferromagnets with DMI, the magnetization at the edges experiences an in-plane tilt due to the boundary conditions imposed by the DMI. In the case of a nanowire along the  $x$ -axis, the magnitude of  $m_x$  due to edge magnetization tilting is given by  $m_x = L\frac{D}{2A}$  where  $L$  is the DW length,  $D$  is the DMI energy per unit area and  $A$  is the exchange stiffness [27–29]. By lowering the PMA, thus increasing  $L$ ,  $m_x$  is increased even further. More importantly, the DMI-induced edge tilting has a chirality and produces a  $m_x$  that is opposite in direction for the two SAF-coupled magnetic layers. This conveniently enables the magnetization of both SAF-coupled layers to be switched simultaneously using SOT, without requiring any bias field.

Figure 1(a) shows a SAF nanowire with the left and right halves having an anisotropy energy density of 300 and 600 kJ m<sup>-3</sup>, respectively. Such localized reduction in PMA can be achieved experimentally by using a combination of ion implantation and lithography processes [30, 31]. Even though the magnetization of the top and bottom layers is opposite, the effective field from the spin Hall effect ( $\vec{H}_{SH}$ ) always act to reverse the magnetization at the edges. Furthermore, the lowered PMA allows  $\vec{H}_{SH}$  to switch the magnetization without needing a high current density. Figure 1(b) shows that after nucleation of the first DW, it is driven to the right into the region of higher PMA by the spin Hall effective field. The magnetization at the left edge will tilt again when the DW is driven sufficiently far, and the cycle can be repeated indefinitely for continuous domain nucleation. (supplementary video 1 is available online at [stacks.iop.org/NJP/20/013029/mmedia](https://stacks.iop.org/NJP/20/013029/mmedia).)

### 4. Three terminal skyrmion device

To circumvent the topological protection of a skyrmion, the magnetization reversal process should be initiated at the edges where topological charge can be added without much energy costs [32]. In figure 2(a), we show such a device where skyrmions can be injected via a 20 nm wide branch protruding from the 60 nm wide main nanowire. The limitations of standard fabrication techniques were also taken into consideration by rounding the inner corners of the device. In the branch, the PMA is reduced to take advantage of SOT for efficient in-line domain injection as described earlier. The device is operated by the application of pulsed current at each of the three terminals. To write a skyrmion, a positive voltage is applied to  $V_2$  and  $V_3$  while keeping  $V_1$  grounded. Due

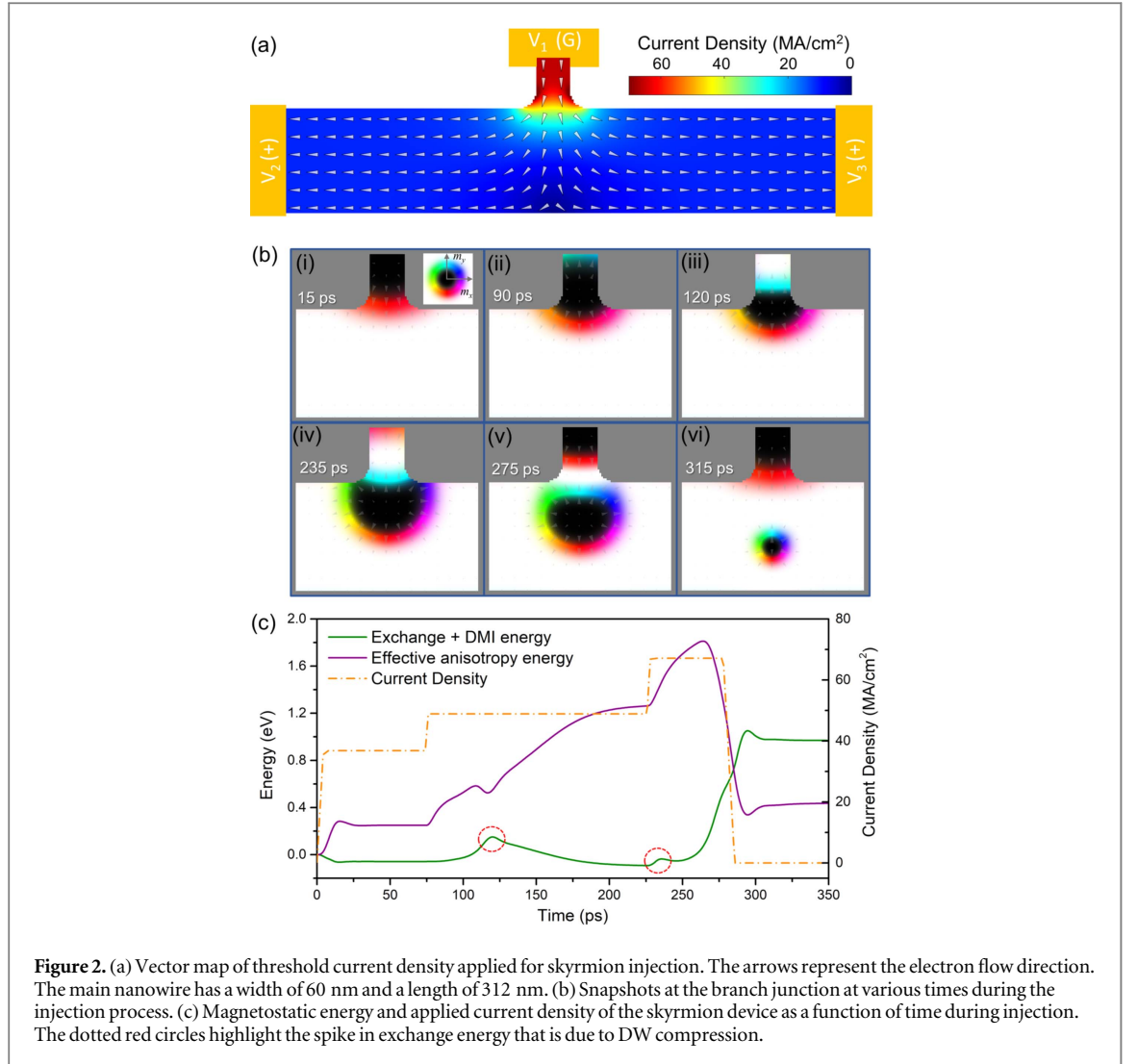


**Figure 2.** (a) Vector map of threshold current density applied for skyrmion injection. The arrows represent the electron flow direction. The main nanowire has a width of 60 nm and a length of 312 nm. (b) Snapshots at the branch junction at various times during the injection process. (c) Magnetostatic energy and applied current density of the skyrmion device as a function of time during injection. The dotted red circles highlight the spike in exchange energy that is due to DW compression.

to the small width (20 nm) of the nanowire branch, a high current density is experienced within the branch which conveniently allows rapid domain nucleation and thus skyrmion injection into the main nanowire.

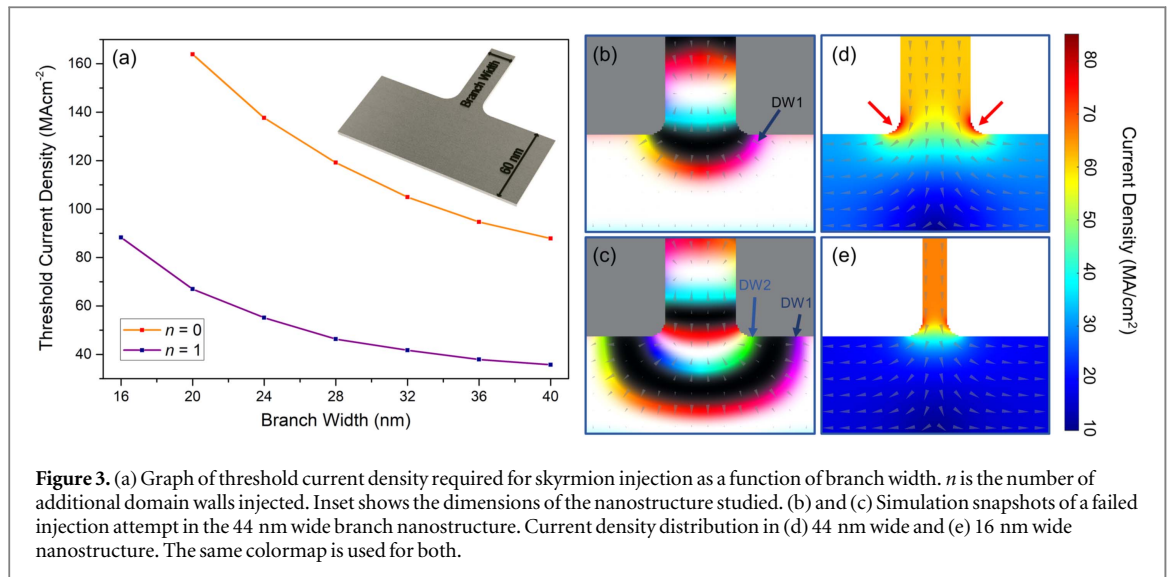
The skyrmion injection process can be summarized as the nucleation of two DWs, followed by their depinning at the branch junction. During the process the two DWs wrap around to form a single skyrmion. Under a current density of  $67 \text{ MA cm}^{-2}$ , skyrmions are nucleated in less than 100 ps. To analyze the nucleation process and observe the depinning mechanisms, the current density is increased in smaller steps. The simulation snapshots at various times of interest are shown in figure 2(b). Applying a current density of  $36 \text{ MA cm}^{-2}$ , the DMI-induced edge magnetization tilting allows the SOT to nucleate a DW, in the same way as shown in figure 1. However, at the junction, there is a strong pinning field attributable to two sources. Firstly, the higher PMA in the nanowire, and secondly, the energy needed for DW bending and stretching. The latter can be seen from the crescent DW shape in the magnetization profile at the 15 ps snapshot. Without a higher current density, the DW remains pinned.

Since the skyrmion injection process involves the nucleation and propulsion of DWs, the magnetostatic energy of the system can be understood from the DW areal energy density given by [33, 34],

$$\sigma = \frac{2A}{L} + 2K_{\text{eff}}L - D\pi, \quad (1)$$

where  $K_{\text{eff}}$  is the effective anisotropy considering the demagnetizing fields. When the DW is compressed, the exchange energy is increased at the expense of the anisotropy. The interplay between the two energies therefore signals any change in DW length. The magnetostatic energy of the system with respect to time is shown in figure 2(c).

At 70 ps, the current density is increased to  $49 \text{ MA cm}^{-2}$  which is sufficient for the nucleation of the second DW. As the second DW is pushed downwards, it interacts repulsively with the first DW which is apparent from

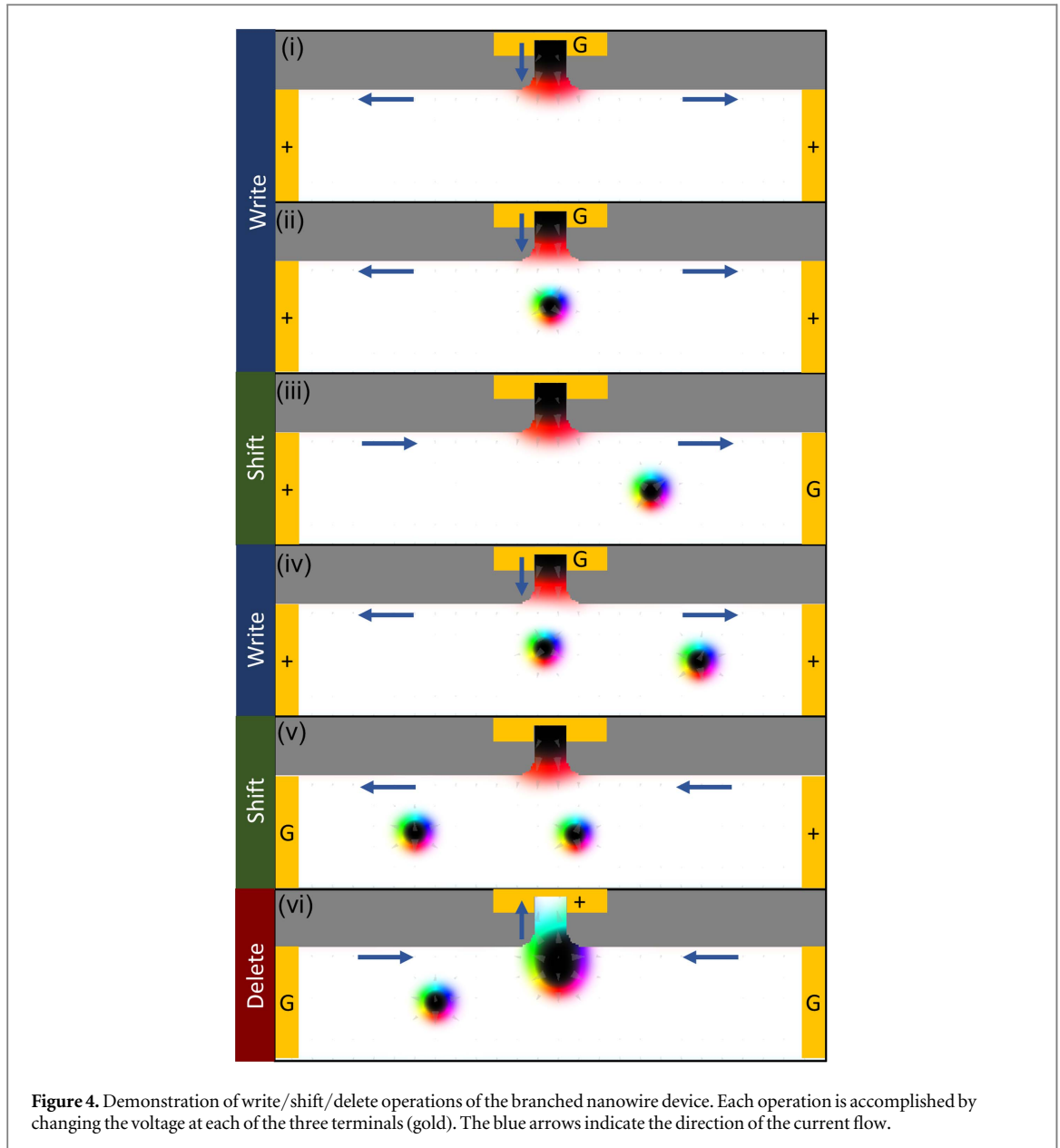


the spike in the exchange energy and the fall in anisotropy energy. However, the pinning potential experienced by the first DW is still stronger than sum of the SOT force and repulsive interaction force received. With the final increase of current density to  $67 \text{ MA cm}^{-2}$ , an immediate spike in exchange energy is observed. This is explained by the second DW exerting an additional pressure on the first, due to the second DW experiencing the increased push from the SOT. At 275 ps, a third DW is nucleated which provides the last push required to depin the first two DWs from the junction and a skyrmion is expelled.

From the skyrmion injection process, it is apparent that the cumulative DW pressure helps to reduce the threshold injection current. Next, we investigated if the addition of extra DW ( $n$ ) in the branch lowers the threshold injection current. By increasing or decreasing the anisotropy value in the top most edge of the branch, the SOT-induced DW nucleation is toggled on or off. With only two DWs ( $n = 0$ ), the minimum required for skyrmion formation, the threshold injection current density was found to nearly triple to  $163 \text{ MA cm}^{-2}$  as compared to the case of one additional DW ( $n = 1$ ). Although more DWs can be added to the DW chain to further reduce the threshold skyrmion nucleation current density, it is necessary to increase the length of the branch to accommodate additional DWs. Unfortunately, this increases the electrical resistance of the branch and offsets the gain in efficiency from the reduced threshold current density.

The dependence of the threshold injection current density on the branch width was also investigated. Increasing the branch width, the threshold injection current density was found to decrease, as shown in figure 3(a). However, there exists a limit for the maximum branch width. At widths of more than 40 nm, the first DW (DW1) depins much earlier than the second DW (DW2). Consequently, the two DWs do not join to form a skyrmion as shown in figures 3(b) and (c). This phenomenon can be understood from the current density distribution where most of the current is concentrated at the branch corners as highlighted in figure 3(d). Therefore, in wide branches, DWs are depinned more easily. On the other hand, branches that are narrower than 16 nm have a relatively uniform current density and do not suffer from this mode of failure. Instead, the narrower branches cause the main nanowire to receive a lower amount of current. Therefore, when the first DW is pushed into the main nanowire, it no longer receives a strong propagation force. As a result, the DWs in a narrow branch require an unrealistically high current density to depin.

The branched nanowire geometry is not only able to achieve efficient skyrmion injection, but it also allows for bit shift and delete operations. By changing the pulse amplitudes of  $V_{1-3}$ , the write, shift, and delete operations can be performed. In figure 4, we demonstrate the writing of two skyrmions followed by a shift operation and finally the deletion of the first skyrmion. While the nucleation and manipulation of only two skyrmions was demonstrated, the proposed device has a storage capacity that is similar to the well-studied skyrmion racetrack memory devices [1, 2, 5, 7, 12, 35]. Skyrmion shifting is achieved by the application of a current density along the axis of the nanowire. The delete operation is the reverse of the write operation; instead of pushing out a skyrmion, the skyrmion is instead drawn towards the branch where it eventually annihilates. For the shift and delete operations, the threshold current density is less than  $20 \text{ MA cm}^{-2}$  which is significantly less than the threshold skyrmion injection current. The difference is due to the reduced pinning force as it is energetically favorable for skyrmions to move from the high PMA nanowire into the low PMA branch. The entire process outlined in figure 4 is shown in supplementary video 2.

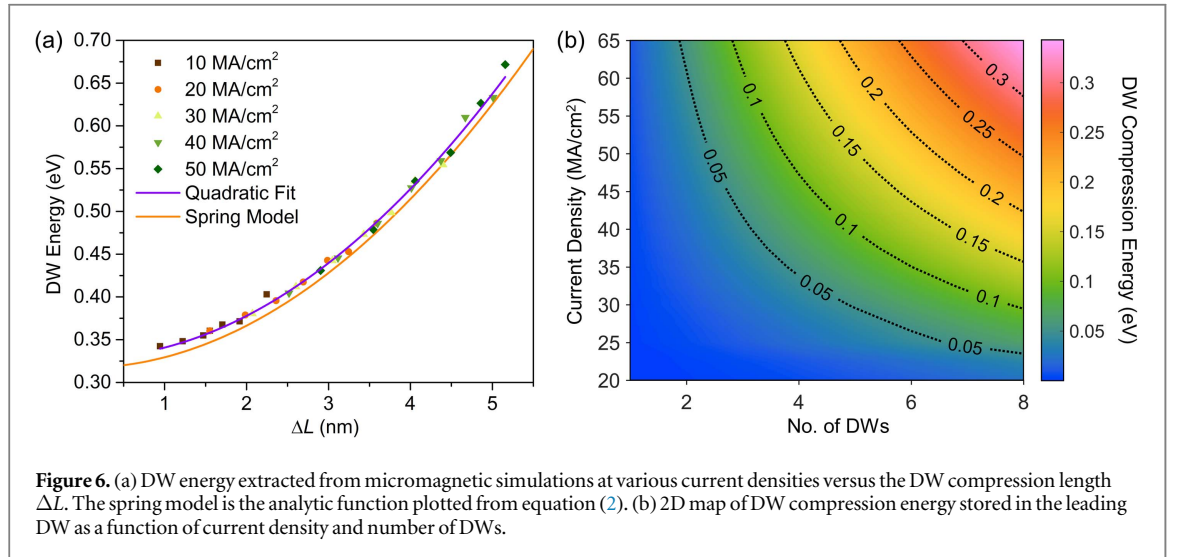
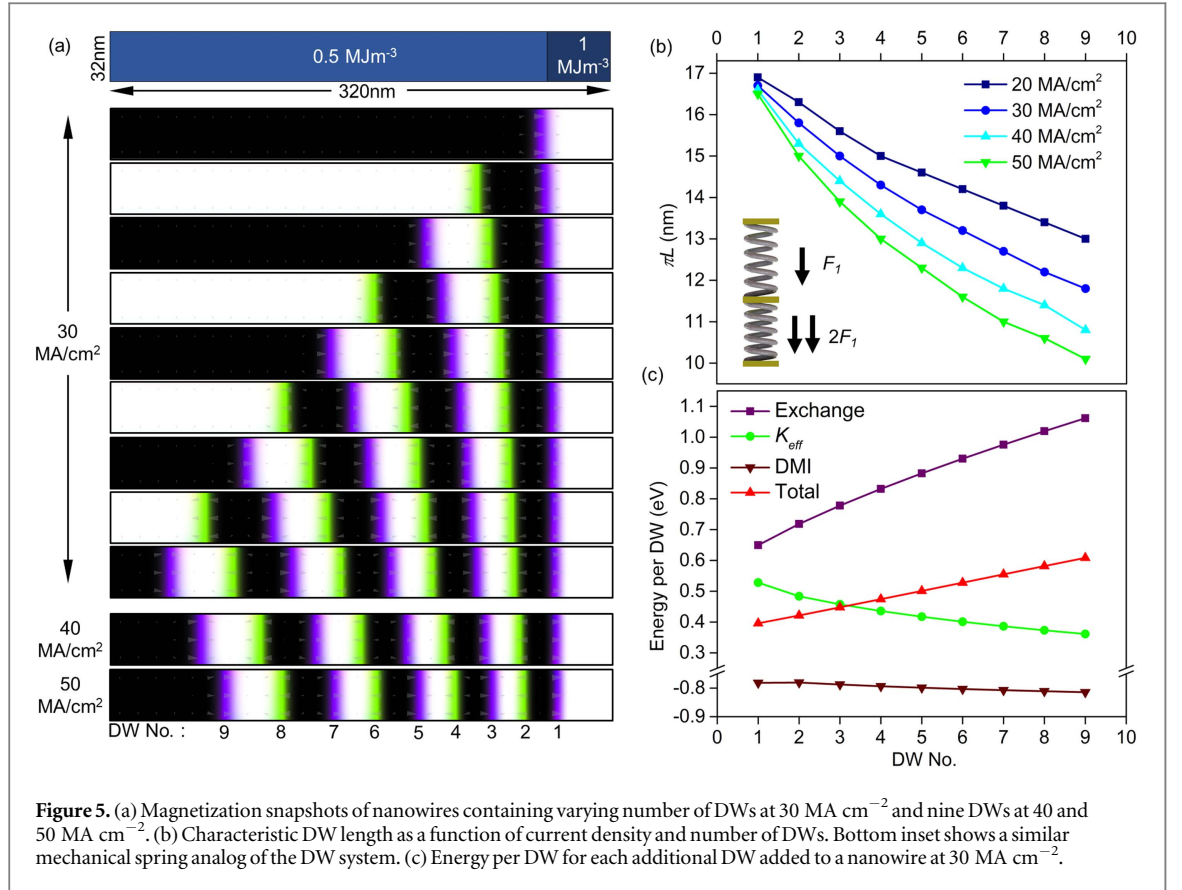


## 5. Increased spin torque efficiency in a DW chain

The DW magnetization profile was studied as a function of the number of DWs in the chain. A SAF nanowire with an anisotropy step was considered as shown in figure 5. The anisotropy step represents an energy barrier that pins the leading DW if insufficient SOT is supplied. Under a current density of  $30 \text{ MA cm}^{-2}$ , the number of DWs in the chain was gradually incremented. Figure 5(a) shows the equilibrium magnetization configuration. As more DWs were added, the leading DWs becomes increasingly compressed. Unsurprisingly, when increasing the current density to 40 and  $50 \text{ MA cm}^{-2}$ , the DW chain compression also increases. It can be concluded that the compression arises from the SOTs experienced by the DWs.

By calculating the DW length from micromagnetic simulations, the DW compression can be quantified (see methods). In figure 5(b), an increase in current density compresses each DW in the chain non-uniformly, with the first DW experiencing the most compression and slight less for each DW that follows. This suggests that each DW up the chain experiences the cumulative force that acts on the previous DWs. Figure 5(c) shows the magnetostatic energy of each DW in the system. As the DWs become increasingly compressed, anisotropy energy is decreased. However, the energy change is offset by the increase in exchange energy, resulting in a net linear increase of energy in the system. The change in magnetostatic energy is consistent with the DW areal energy density given by equation (1).

Néel DWs are known to tilt when a SOT effective field is applied. However, in a SAF nanowire, the tilt of the top and bottom DWs cancels out and results in a DW with no tilt [36]. Therefore, the SAF DW chain system is



reminiscence of a vertical stack of mechanical springs; each spring experiences a gravitational force  $F_1$  and the gravitational force from all the springs above, culminating in the bottom most spring acquiring the most compression energy. Substituting the equilibrium DW length  $L_{eq} = \sqrt{\frac{A}{K_{eff}}}$  into equation (1), the Maclaurin's series read:

$$\sigma(\Delta L) = \sigma_{eq} + 2\sqrt{\frac{K^3}{A}} \Delta L^2 + O(\Delta L^3), \quad (2)$$

where  $\Delta L$  is the change in DW length caused by the compression and  $\sigma_{eq}$  is the DW energy at equilibrium which is calculated to be 0.317 eV for the geometry and material parameters used in our study. In figure 6(a), we show that the spin torque-induced DW compression can indeed be modeled like the compression of a mechanical spring; in the form of a quadratic relation between energy stored and compression length using equation (2). The

slight  $y$  offset between the analytical and numerical data can be explained by the DWs experiencing a DMI-induced edge tilting along the  $y$ -axis which results in increased anisotropy energy. Nonetheless, the energy offset is less than 5%. The coefficient of the quadratic term was also found to be different by no more than 1%. The surprisingly good fit between the numerical data and our spring model demonstrates that the energy changes due to the application of spin torques can be completely accounted for by DW compression.

Under a spin torque compression, the DWs accumulate energy which is then used to overcome pinning potentials. With a quadratic spring model, it becomes possible to obtain the compression energy of the DWs using only the changes in DW lengths. The compression energy of the leading DW was obtained as a function of applied current density and number of DW in the chain, as shown in figure 6(b). The compression energy was found to scale linearly with both the current density and number of DWs. The number of DWs therefore acts as a multiplier to the amount of spin-torque experienced by the leading DW. As a result, the combination of a high current density and a long DW chain can produce a compression energy that is useful for overcoming pinning potentials.

## 6. Conclusion

In this paper, we have demonstrated a highly efficient in-line skyrmion injection method using a branched nanowire geometry in a synthetic antiferromagnet system. The exploitation of the DMI-induced edge tilting and efficient SOTs allowed DWs to be injected efficiently into the branch. Further accumulating DWs in the branch created a compression of the leading DW, which provides the required energy to depin the DWs from the junction. The compression mechanism resulted in the reduction of the threshold injection current density by a third. The branched device also functions as a skyrmion memory cell that uses only three terminals to accomplish the shift/delete/write operations. Lastly, we have also investigated the DW compression and found that the DW chain acts like a mechanical spring when compressed. This discovery reduces the depinning current density in DW logic and memory devices, thus improving energy efficiency.

## Acknowledgments

The work was supported by the Singapore National Research Foundation, Prime Minister's Office under a Competitive Research Programme (Non-volatile Magnetic Logic and Memory Integrated Circuit Devices, NRF-CRP9-2011-01), and an Industry-IHL Partnership Program (NRF2015-IIP001-001). The support from an RIE2020 AME-Programmatic Grant (No A1687b0033) is also acknowledged. WSL is also a member of the Singapore Spintronics Consortium (SG-SPIN).

## Author contributions

WLG proposed the idea and designed the micromagnetic model. WLG and SK performed the micromagnetic simulations and WLG analyzed the data. The study was supervised by WSL. All authors contributed to the discussion and preparation of the manuscript.

## Competing financial interests

The authors declare no competing financial interest.

## ORCID iDs

W L Gan  <https://orcid.org/0000-0001-9278-0718>

## References

- [1] Zhang Y *et al* 2017 Magnetic skyrmion without skyrmion Hall effect in magnetic nanotrack with perpendicular anisotropy *Nanoscale* **9** 10212–18
- [2] Yu G *et al* 2017 Room-temperature skyrmion shift device for memory application *Nano Lett.* **17** 261–8
- [3] Fert A, Reyren N and Cros V 2017 Magnetic skyrmions: advances in physics and potential applications *Nat. Rev. Mater.* **2** 17031
- [4] Woo S *et al* 2016 Observation of room-temperature magnetic skyrmions and their current-driven dynamics in ultrathin metallic ferromagnets *Nat. Mater.* **15** 501–6
- [5] Fook H T, Gan W L and Lew W S 2016 Gateable skyrmion transport via field-induced potential barrier modulation *Sci. Rep.* **6** 21099
- [6] Purnama I, Gan W L, Wong D W and Lew W S 2015 Guided current-induced skyrmion motion in 1D potential well *Sci. Rep.* **5** 10620

- [7] Sampaio J, Cros V, Rohart S, Thiaville A and Fert A 2013 Nucleation, stability and current-induced motion of isolated magnetic skyrmions in nanostructures *Nat. Nanotechnol.* **8** 839–44
- [8] Woo S et al 2017 Spin-orbit torque-driven skyrmion dynamics revealed by time-resolved x-ray microscopy arXiv:1705.09019
- [9] Jiang W et al 2017 Direct observation of the skyrmion Hall effect *Nat. Phys.* **13** 162–9
- [10] Zhang X, Zhou Y and Ezawa M 2016 Magnetic bilayer-skyrmions without skyrmion Hall effect *Nat. Comms.* **7** 10293
- [11] Zhang X et al 2015 Skyrmion–skyrmion and skyrmion–edge repulsions in skyrmion-based racetrack memory *Sci. Rep.* **5** 7643
- [12] Ding J, Yang X and Zhu T 2015 Manipulating current induced motion of magnetic skyrmions in the magnetic nanotrack *J. Phys. D: Appl. Phys.* **48** 115004
- [13] Koshibae W and Nagaosa N 2017 Theory of skyrmions in bilayer systems *Sci. Rep.* **7** 42645
- [14] Kim D H, Moon K W, Yoo S C, Min B C, Shin K H and Choe S B 2013 A method for compensating the Joule-heating effects in current-induced domain wall motion *IEEE Trans. Magn.* **49** 3207–10
- [15] Curiale J, Lemaitre A, Niazi T, Faini G and Jeudy V 2012 Joule heating and current-induced domain wall motion *J. Appl. Phys.* **112** 103922
- [16] Kim K-J, Lee J-C, Choe S-B and Shin K-H 2008 Joule heating in ferromagnetic nanowires: prediction and observation *Appl. Phys. Lett.* **92** 192509
- [17] Yamaguchi A et al 2005 Effect of Joule heating in current-driven domain wall motion *Appl. Phys. Lett.* **86** 012511
- [18] Li S, Goolaup S, Kwon J, Luo F, Gan W and Lew W S 2017 Deterministic spin-orbit torque induced magnetization reversal in Pt/[Co/Ni]<sub>n</sub>/Co/Ta multilayer Hall bars *Sci. Rep.* **7** 972
- [19] Engel C, Goolaup S, Luo F, Gan W and Lew W S 2017 Spin-orbit torque induced magnetization anisotropy modulation in Pt/(Co/Ni)<sub>4</sub>/Co/IrMn heterostructure *J. Appl. Phys.* **121** 143902
- [20] Zhang C, Fukami S, Sato H, Matsukura F and Ohno H 2015 Spin-orbit torque induced magnetization switching in nano-scale Ta/CoFeB/MgO *Appl. Phys. Lett.* **107** 012401
- [21] Fan Y et al 2014 Magnetization switching through giant spin-orbit torque in a magnetically doped topological insulator heterostructure *Nat. Mater.* **13** 699–704
- [22] Cubukcu M et al 2014 Spin-orbit torque magnetization switching of a three-terminal perpendicular magnetic tunnel junction *Appl. Phys. Lett.* **104** 042406
- [23] Martinez E, Emori S and Beach G S D 2013 Current-driven domain wall motion along high perpendicular anisotropy multilayers: the role of the Rashba field, the spin Hall effect, and the Dzyaloshinskii–Moriya interaction *Appl. Phys. Lett.* **103** 072406
- [24] Oh Y W et al 2016 Field-free switching of perpendicular magnetization through spin-orbit torque in antiferromagnet/ferromagnet/oxide structures *Nat. Nanotechnol.* **11** 878–84
- [25] Lau Y C, Betto D, Rode K, Coey J M and Stamenov P 2016 Spin-orbit torque switching without an external field using interlayer exchange coupling *Nat. Nanotechnol.* **11** 758–62
- [26] Yu G et al 2014 Switching of perpendicular magnetization by spin-orbit torques in the absence of external magnetic fields *Nat. Nanotechnol.* **9** 548–54
- [27] Han D S et al 2016 Asymmetric hysteresis for probing Dzyaloshinskii–Moriya interaction *Nano Lett.* **16** 4438–46
- [28] Pizzini S et al 2014 Chirality-Induced asymmetric magnetic nucleation in Pt/Co/AlO<sub>x</sub> ultrathin microstructures *Phys. Rev. Lett.* **113** 047203
- [29] Rohart S and Thiaville A 2013 Skyrmion confinement in ultrathin film nanostructures in the presence of Dzyaloshinskii–Moriya interaction *Phys. Rev. B* **88** 184422
- [30] Devolder T et al 1999 Patterning of planar magnetic nanostructures by ion irradiation *J. Vac. Sci. Technol. B* **17** 3177
- [31] Devolder T et al 1999 Sub-50 nm planar magnetic nanostructures fabricated by ion irradiation *Appl. Phys. Lett.* **74** 3383–5
- [32] Cortes-Ortuno D et al 2017 Thermal stability and topological protection of skyrmions in nanotracks *Sci. Rep.* **7** 4060
- [33] DeJong M D and Livesey K L 2017 Domain walls in finite-width nanowires with interfacial Dzyaloshinskii–Moriya interaction *Phys. Rev. B* **95** 054424
- [34] DeJong M D and Livesey K L 2015 Analytic theory for the switch from Bloch to Néel domain wall in nanowires with perpendicular anisotropy *Phys. Rev. B* **92** 214420
- [35] Tomasello R et al 2017 Performance of synthetic antiferromagnetic racetrack memory: domain wall versus skyrmion *J. Phys. D: Appl. Phys.* **50** 325302
- [36] Krishnia S et al 2017 Role of RKKY torque on domain wall motion in synthetic antiferromagnetic nanowires with opposite spin Hall angles *Sci. Rep.* **7** 11715
- [37] Vansteenkiste A, Leliaert J, Dvornik M, Helsen M, Garcia-Sanchez F and Van Waeyenbergh B 2014 The design and verification of MuMax3 *AIP Adv.* **4** 1107133
- [38] Grytsyuk S et al 2016 k-asymmetric spin-splitting at the interface between transition metal ferromagnets and heavy metals *Phys. Rev. B* **93** 174421